



LAWRENCE
LIVERMORE
NATIONAL
LABORATORY

Smart Tracers for Geothermal Reservoir Assessment

W. DuFrance, J. Vericella, E. Duoss, M. Smith, R. Aines, J. Roberts

May 9, 2014

38th Annual Meeting, Geothermal Resource Council
Portland, OR, United States
September 28, 2014 through October 1, 2014

Disclaimer

This document was prepared as an account of work sponsored by an agency of the United States government. Neither the United States government nor Lawrence Livermore National Security, LLC, nor any of their employees makes any warranty, expressed or implied, or assumes any legal liability or responsibility for the accuracy, completeness, or usefulness of any information, apparatus, product, or process disclosed, or represents that its use would not infringe privately owned rights. Reference herein to any specific commercial product, process, or service by trade name, trademark, manufacturer, or otherwise does not necessarily constitute or imply its endorsement, recommendation, or favoring by the United States government or Lawrence Livermore National Security, LLC. The views and opinions of authors expressed herein do not necessarily state or reflect those of the United States government or Lawrence Livermore National Security, LLC, and shall not be used for advertising or product endorsement purposes.

Smart Tracers for Geothermal Reservoir Assessment

Wyatt Du Frane, John Vericella, Eric Duoss, Megan Smith, Roger Aines, Jeff Roberts

Lawrence Livermore National Laboratory

Keywords: tracers, encapsulated tracers, smart tracers, temperature profiles

Paper Topic: Exploration / Resource Assessment / Management

Abstract

We have developed a method of manufacturing and testing “smart” encapsulated tracers that release at specified temperatures. These encapsulated tracers can be used to simultaneously map both flowfield distributions and flowpath-specific temperature within a reservoir. Here we report on the methods of fabrication and initial tests of durability, obtaining release as a function of temperature, and flow through replicated rock fractures. The tracer capsules were created as double emulsions, using microfluidic techniques, with 4 wt% fluorescein solution inside shells formed from commercially available materials. The smart tracer capsules were subjected to several geothermal temperatures in internally pressurized, externally heated vessels for durations of 2 to 16 hours. Fluorescein contents in the surrounding fluid were measured afterwards with UV-Vis to quantify encapsulated tracer release. Capsules of one shell material displayed significant fluorescein release at temperatures as low as 80 °C, while capsules made from another shell material showed tracer release over a much higher and narrower temperature range (160 – 200 °C). The fluorescein tracer itself also underwent substantial degradation over times > 2 hours at 200 °C. To validate the transport of these encapsulated tracers, natural rock fracture surfaces were duplicated via 3-D printing techniques to form a transparent flow cell. Smart tracers were pumped through the flow cells at a variety of fluid velocities to verify that they can be easily transported into fracture systems. These initial tests demonstrate the ability to manufacture encapsulated tracers capable of tracer release at temperatures above a specified threshold, and rugged enough to survive pumping and transport through a fracture.

Introduction

Geothermal energy is a potentially large source for clean domestic energy, but has historically been limited to regions with shallow magmatism near tectonic plate boundaries. Fluids are injected deep into formations and recovered at higher temperatures to produce energy (Figure 1). If geothermal energy were economically viable in more locations, it could potentially produce vast amounts of renewable energy to and reduce U.S. dependency on foreign oil, but improved data collection techniques would be necessary to engineer geothermal fields to that level of production. Tracers are widely used by industry to map flow distributions and optimize well placement, by injecting them and monitoring their breakthrough at production wells (Figure 2a-c). Suitable tracers are materials or chemicals that are easily detectable in trace amounts, and in the case of geothermal use, these compounds must also persist over long time periods during prolonged exposure to harsher deep subsurface conditions. A variety of tracers have been proposed for use in geothermal wells (e.g., Dennis et al., 1981; Gunderson et al., 2002; Alaskar et al., 2012; Nottebohm et al., 2012).

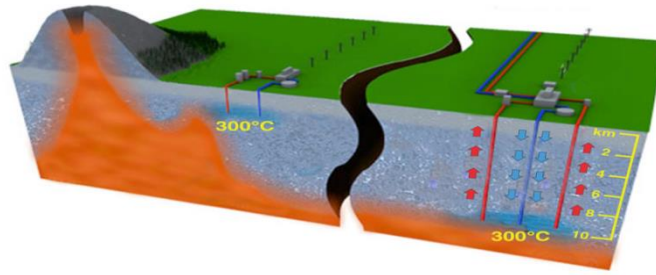


Figure 1. Schematic of a successfully operating geothermal field. Fluid is injected into natural or engineered fracture networks through thermal formations and recovered at higher temperature, producing a positive net energy gain (Tester et al., 2006; figure from www.geothermalanywhere.com).

If tracers could be designed to react or release at specific temperatures, they could be used simultaneously to map flow and temperature distributions in the field (e.g., Figure 2d). This information would be beneficial for assessing both natural and engineered fracture networks for their geothermal energy production capabilities. The capability to encapsulate one common tracer compound, fluorescein, using double emulsion techniques (e.g. Shah et al. 2008) has been previously verified by the LLNL additive manufacturing lab (Figure 3). Here we report the results of a feasibility study focused on three aspects of encapsulated tracer technology: 1) manufacturing methods, including material selections and size uniformity; 2) mechanical integrity of smart tracer capsules with hydraulic pumps and fracture flow; and 3) design and control of triggered capsule “release” of tracer fluids at geothermally relevant temperatures. (~200 °C).

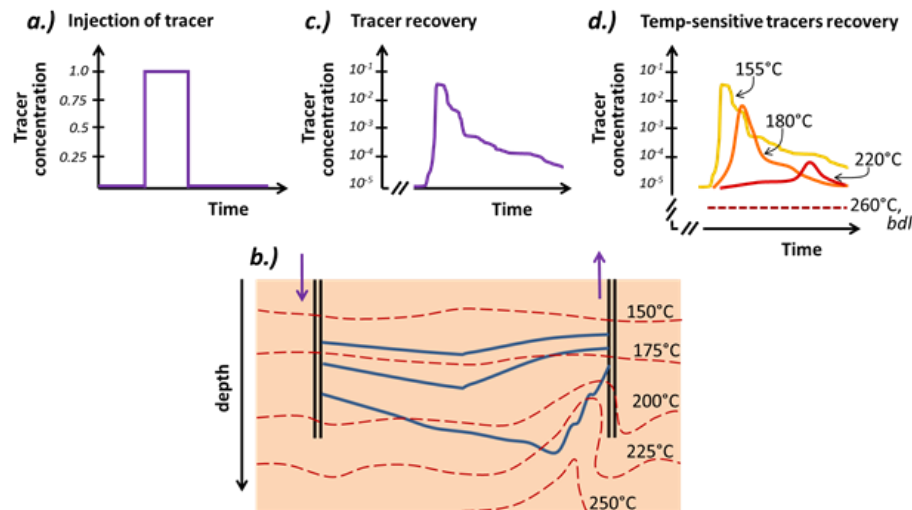


Figure 2: Tracer injection (a) into the subsurface can follow multiple pathways shown in blue, and encounter different temperature zones shown as red dashed lines (b). While conventional conservative tracer recovery (c) yields only flowpath information, the “smart” tracers we propose will help map the temperature distributions along flow pathways within the production volume (d). In this schematic, we envision the use of four distinct tracers, encapsulated in shell materials capable of release at different “target” temperatures (155, 180, 220, and 260°C). Note that 260°C-targeted tracer remains below detection limit for all given flowpaths.

Experimental Methods

Double emulsions were created using capillary microfluidic devices and then exposed to ultraviolet (UV) radiation, polymerizing the outer droplet to form a solid capsule wall around the encapsulated inner fluid (4 wt% fluorescein in aqueous solution; Figure 3). To create the microfluidic flow-focusing devices, we first pulled-down circular glass capillaries in a pipette puller to create a tapered end. This tapered capillary was inserted into a square capillary with an inner dimension which roughly matches the outer diameter of the circular tapered capillary. A second circular capillary (not tapered) was inserted into the opposite end of the square capillary and brought into close proximity of the end of the tapered capillary. All of the capillaries were affixed with epoxy onto a large glass substrate with careful control over the alignment of the capillaries. In this configuration, the core fluid containing the tracer flows through the tapered capillary, the middle or shell fluid flows between the interstitial space between the circular tapered capillary and the square capillary, and carrier fluid flows in the interstitial space between the non-tapered circular capillary and the square capillary. Flow rates of the core fluid, shell fluid, and carrier fluid were tuned to create double emulsions. Emulsions were collected in a surfactant solution surfactant (Pluronic F127, BASF) and spun gently in sealed vials under UV light to fully polymerize shell materials. Two commercially available photocurable polymers were used to form capsule shells: “E-MAX” (Dymax Inc., Torrington, CT) and Norland Optical Adhesive 61, and “NOA” (Norland Products, Cranburg, NJ). The E-MAX shell material has a vivid blue fluorescence when exposed to UV light (365 nm) and is easily cured within several seconds. The second material, NOA 61, is commonly used for optical applications at temperatures up to 125 °C, and is curable under UV light with absorption between 320-380 nm with maximum peak sensitivity at 365 nm.

Flow cells were created to visualize particle interactions with rock fracture surfaces. A fractured core sample of Marcellus shale was provided by National Energy Technology Laboratory (NETL). The roughly planar, 45x45 mm² fracture was oriented perpendicular to bedding and was partially lined with calcite. The fractured sample was first imaged using x-ray computed microtomography, and then the fracture was fully opened using the Brazilian test fracturing method by applying a tangential force (work performed by NETL, Figure 4a). Profilometry measurements (Nanovea, Irvine, CA) were performed on the open surfaces of the fracture using a non-contact ST400 Optical Profiler (Figure 4b). The fracture surface images were then recreated using high resolution 3-D printing to form a flow cell in transparent plastic (DSM’s Somos® WaterShed, Figure 4c). The two halves of the fracture flow cell were offset by gaskets of variable thicknesses, effectively setting the fracture aperture. The cell was clamped with bolts, and fitted with Luer lock connections at the outlet and inlet (Figure 5). The outlet and inlet were then plumbed to 60-mL syringes. Injection from the inlet syringe was controlled by a Harvard PhD 2000 pump. Similar tomography and profilometry data from a 10x30 mm² fractured greywacke sample were also used to make a smaller fracture flow cell for some preliminary tests.

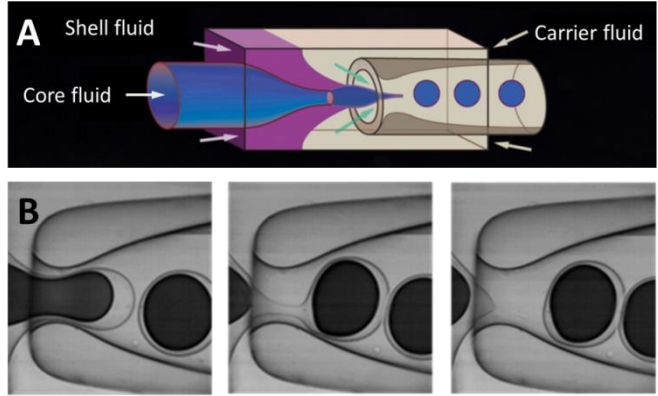


Figure 3: A) Schematic of Schematic illustration of flow-focusing microfluidic device for tracer encapsulation.. B) Time sequence photographs of device and double emulsion formation. Dark droplets are the aqueous core fluid, while the surrounding outline is a liquid photopolymer that will form the microcapsule shell.

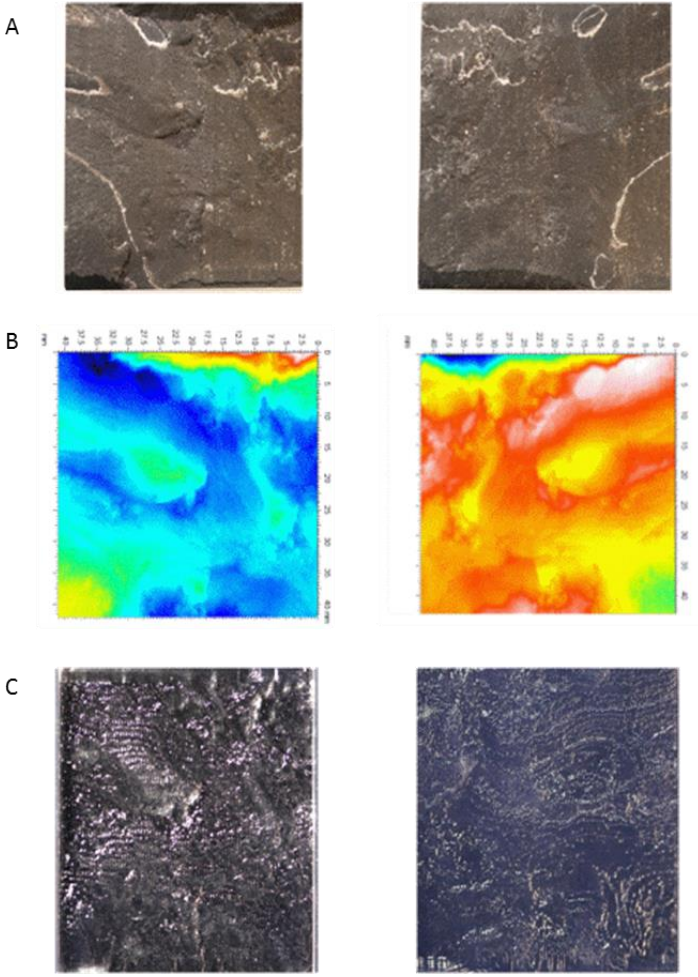


Figure 4: A) Photographs of two complementary fracture surfaces in a Marcellus shale core. B) Profilometry of these surfaces. C) Photographs of the 3D-printed fractures constructed of transparent plastic with 50 μm layer resolution.

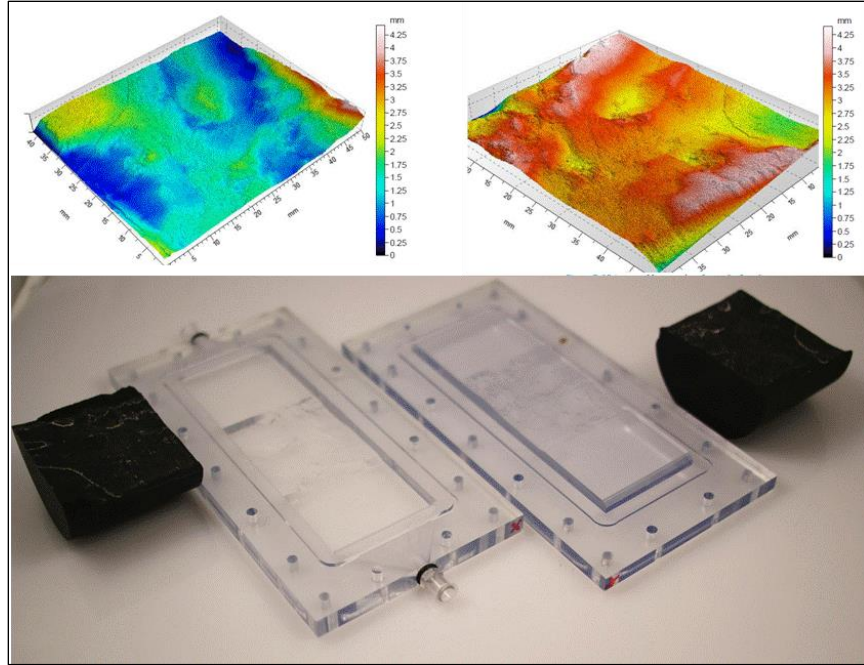


Figure 5: The rock surfaces (characterized by profilometry, above) were recreated by 3-D printing them into a transparent flow cell (below) for visualization of capsule interactions with topological fracture features.

Batch microcapsule release tests were performed at temperatures between 80-200 °C, for durations between 2-16 hours using internally pressurized vessels with PTFE liners (Parr vessels, model 4749). Microcapsules (0.10 +/- 0.05 g) were pipetted into 20g of water and mixed. Initial background samples were collected by removing 10 g of the fluid, leaving the remaining 10g in the vessel with the capsules. Vessels were placed in a box furnace at 80-200 °C for 2-16 hours, and were maintained at steam saturation pressures (Figure 6).

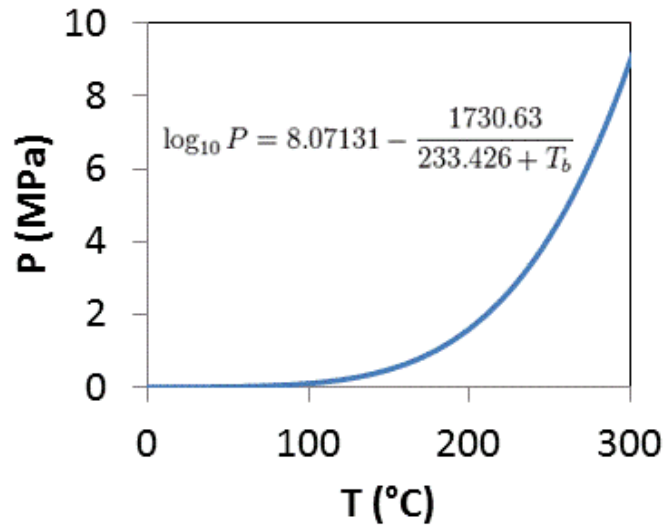


Figure 6: Vapor pressure (P) of water in release tests as a function of temperature (T_b).

Results

Tracer Encapsulation

Fluorescein solution was selected as a tracer solution because it is commonly used in subsurface field tests, and has been previously demonstrated to be compatible with double emulsion techniques. A 4 wt% aqueous fluorescein solution (Sigma Aldrich, St. Louis, MO) was mixed and stored in a lightproof container to minimize photobleaching. To improve contrast for image analysis in some of the tracer delivery experiments, a black dye (1 wt% solution, Brilliant Black BN, Sigma Aldrich, St. Louis, MO) was used as an alternative core solution. Two UV-curable adhesives were used as shell materials.

Capsules were successfully manufactured with average diameters of ~ 0.5 mm and ~ 1.1 g/cm³ densities. The E-MAX shells collapsed after curing but remained impermeable in most cases, whereas the NOA shells remained spherical and intact (Figure 7).

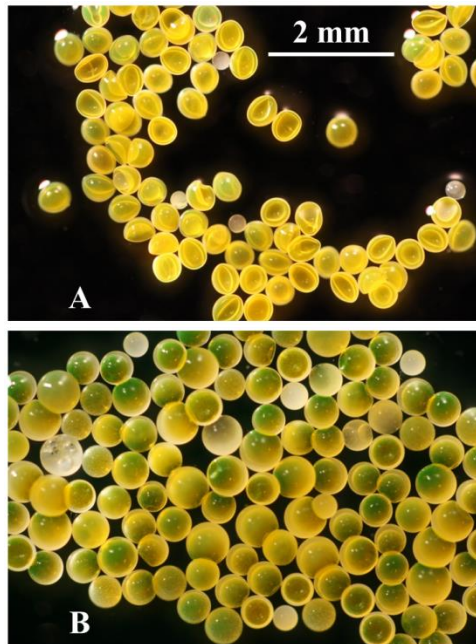


Figure 7: Fluorescein solutions (4 wt% in water) were encapsulated by double emulsion microfluidic devices in either A) E-MAX or B) NOA shell materials.

Tracer Delivery

Tracers with NOA shells were passed through the smaller, preliminary fracture flow cell using multiple gasket thicknesses to prop the fracture open with average apertures of roughly 0.4, 0.8, 1.6, and 2 mm. Tests were performed with the fracture plane oriented horizontally, using fluid velocities between 0.007 and 0.25 m/s. Generally the capsules behaved similarly for all fracture apertures greater than the average capsule diameters (≥ 0.8 mm). For the 0.4 mm fracture aperture, the capsules aggregated at rough and/or small aperture regions, and were frequently observed to dislodge from these areas under increased flow conditions. Capsules

appeared to move via saltation in apertures larger than capsule diameters, especially at the lowest fluid velocities. Increased fluid velocity increased both the frequency with which capsules were entrained in the fluid and the mean travel distance before re-settling.

Tracers with NOA shells containing black dye were flow-tested in the larger Marcellus shale fracture cell. The pumping fluid was ~0.5 wt% Pluronic P-123 solution, to prevent capsules from agglomerating. Tests were performed using a mean fracture aperture of 2.3 mm, with fluid velocities ranging between 8.1×10^{-5} to 1.5×10^{-3} m/s. The fracture plane was oriented both horizontally and vertically (flow introduced from the bottom of the cell). Nylon screen and steel wool frits were installed at the inlet and outlet of the cell to retain capsules within the flow cell. Horizontally oriented tests resulted in similar behavior as in the smaller cell, with capsules flowing across the bottom fracture surface or tumbling over other capsules (saltating). In vertical tests, capsules moved upwards with fluid flow but were observed to cascade downward after interaction with prominent fracture surfaces (Figure 8). For fluid velocities $\geq 5 \times 10^{-4}$ m/s, capsules eventually reached the top of the cell.

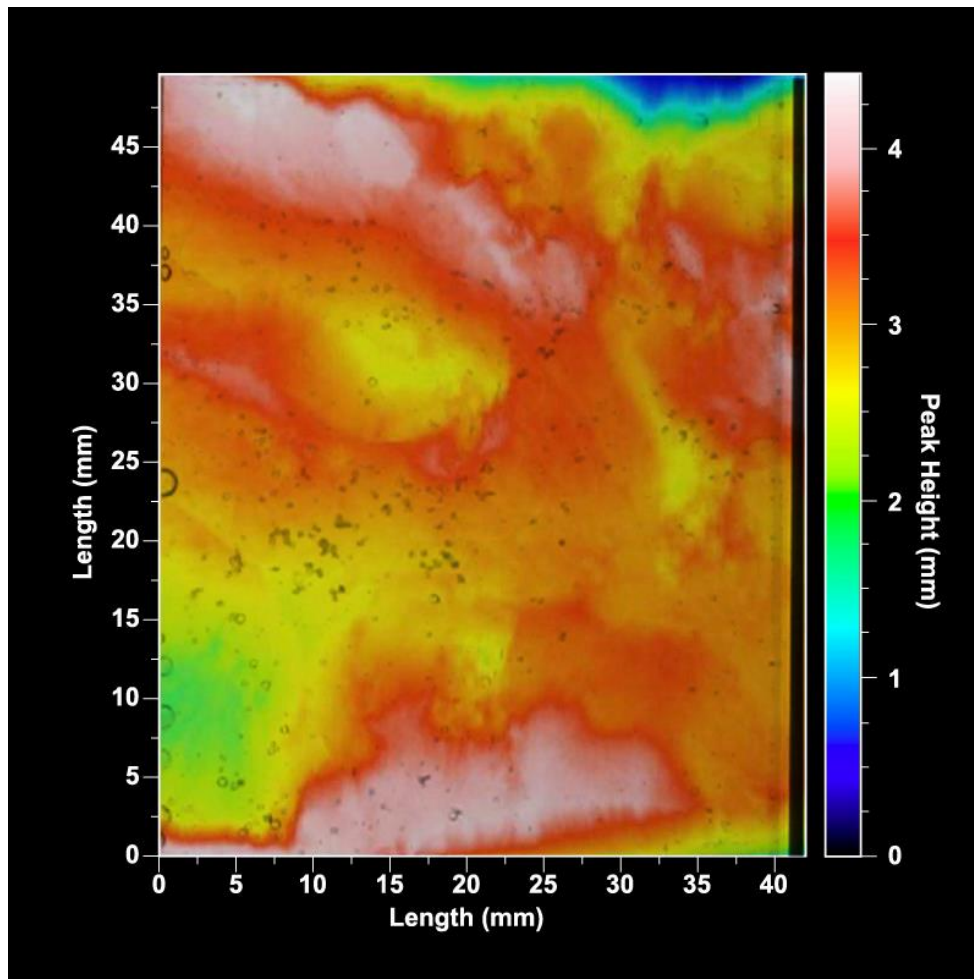


Figure 8: Snapshot of NOA capsules flowing upward in the vertically-oriented fracture cell (fluid velocity $\sim 8.0 \times 10^{-3}$ m/s), with color-mapped profilometry data overlaid. Capsules accumulate at areas of minimum or maximum topology (e.g., at 23-25mm or 35-40mm).

Tracer Release Tests

Capsules containing 4 wt % fluorescein solution in both NOA and E-MAX shells were emplaced in batch reaction vessels with 10g of water, inside a furnace at temperatures of 25, 80, 120, 160, or 200 °C for 2 hours. After 2 hours vessels were taken from the furnace and set on steel plates with copper sheeting to increase cooling rate. Durations reported here include vessel heating time, but not cooling time.

Fluorescein gives water a yellowish tint in both ambient and transmitted light; it fluoresces in ultraviolet light (Figure 9). The E-MAX capsules showed visible signs of fluorescein release for all temperatures (Figure 9a), while fluorescein release was less obvious for the NOA capsules in tests at ≤ 160 °C (Figure 9b). Preliminary tests were also performed at 200 °C on both types of capsules for longer durations (~16 hours). The E-MAX capsules remained intact but became heavily discolored, turning dark brown. The NOA capsules dissolved completely and the surrounding water became cloudy. To determine the time frame over which this dissolution occurs, NOA capsules were heat-treated at 200 °C for 2, 4, 8, and 16 hours. At 200 °C, the NOA capsules remained somewhat intact for test periods ≤ 4 hours; formed a residue at 8 hours; and completely dissolved with no trace of solids after 16 hours.

Fluorescein concentrations in the surrounding water were measured by UV-Vis spectroscopy, at an absorption maximum at 494 nm. Experiments in which NOA shells dissolved also showed an additional absorption shoulder at 430-450 nm (Figure 10). Aqueous fluorescein concentrations were quantified by absorption at 494 nm with daily spectrophotometer calibration. (Figures 11 and 12). Background concentrations of fluorescein were measured from aliquots taken prior to each run, and were typically low compared to post-run samples. The concentration of fluorescein released from a given weight of capsules, $C_{\text{Fluor.}}$, were corrected for background and dilution using the following equation,

$$C_{\text{Fluor.}} = (C_{\text{sample}} - C_{\text{bkgd}}) * (M_{\text{H}_2\text{O}} / M_{\text{caps}}), \quad (1)$$

where C_{sample} and C_{bkgd} are the fluorescein concentrations measured in the post-run and pre-run samples respectively, M_{caps} is the mass of added capsules, and $M_{\text{H}_2\text{O}}$ is the mass of water added to the vessel.

The E-MAX capsules released between 7-17 ppmw fluorescein during 2-hour tests, with the highest amount released in the 160 °C test. Very little fluorescein (1-4 ppmw) was released from NOA capsules in the 2-hour tests at temperatures < 200 °C; however, they released 29 ppm at 200 °C (Figure 12). Fluorescein release from NOA capsules held at 200 °C also decreased sharply over time (Figure 13). The presence of NOA in solution may react with the fluorescein or alternatively the NOA may interfere with fluorescein measurement by reducing the transparency of the samples. However, Adams and Davis (1991) have also reported that fluorescein degrades at exponential rates in oxygenated waters over 5-40 hours, and this process may also be responsible for the trends in the NOA data.

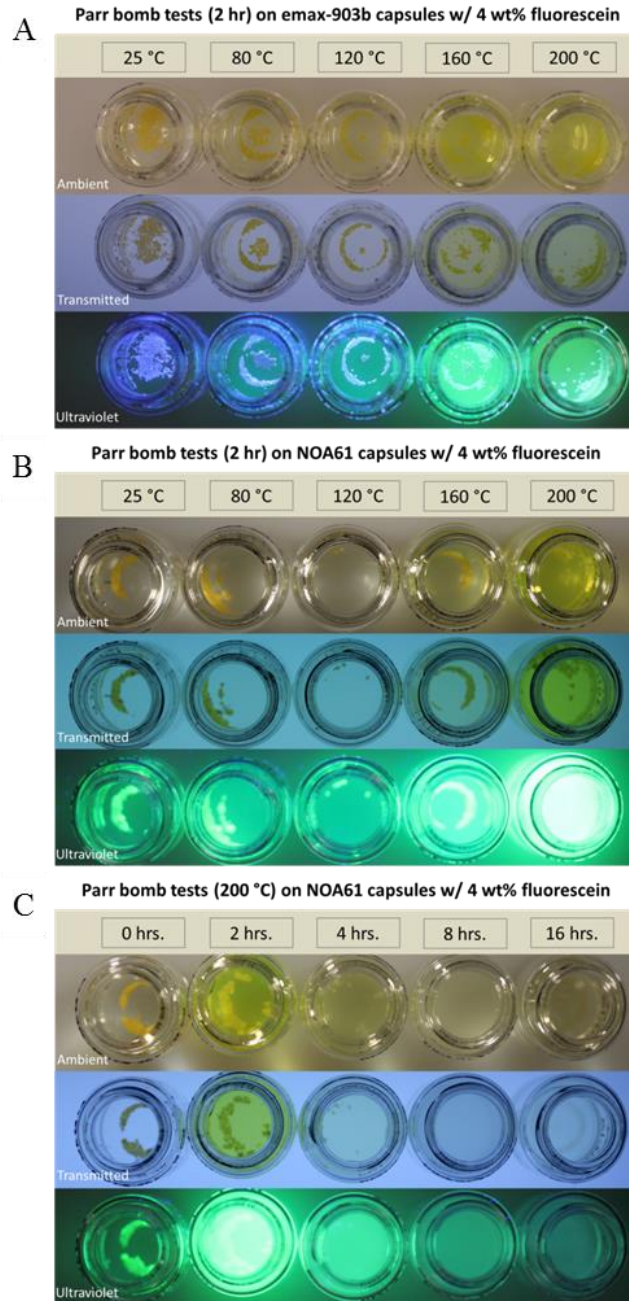


Figure 9: Images of encapsulated tracer subsamples (in 20-mL, 1-in diameter vials) after temperature-release tests in ambient (top row), transmitted (middle row), or ultraviolet light (bottom row of each image). The largest releases of fluorescein occurred at 160 °C for the E-MAX capsules (A), and 200 °C for the NOA capsules (B). Fluorescein also degraded over time > 2 hours at 200 °C (C).

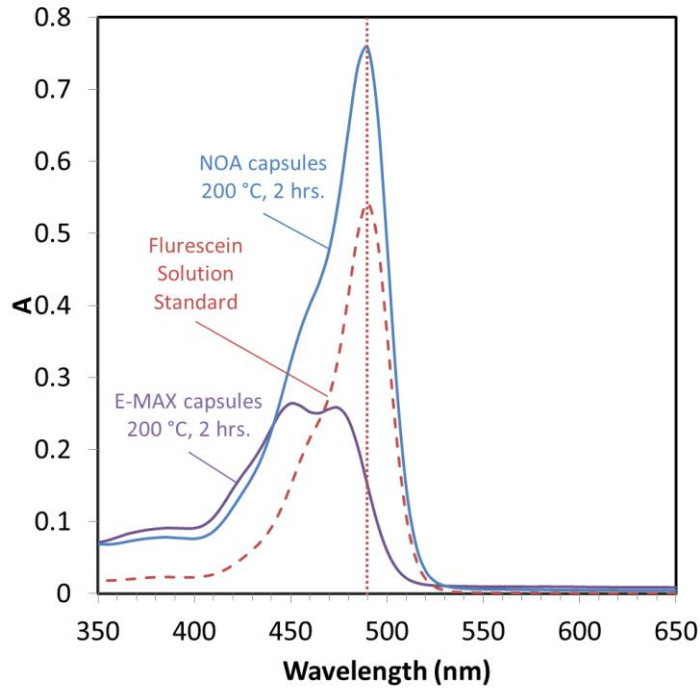


Figure 10: UV-Vis spectra on release test samples in NOA and E-MAX capsules after 200 C exposure for 2 hours, and for a fluorescein solution standard (no temperature exposure).

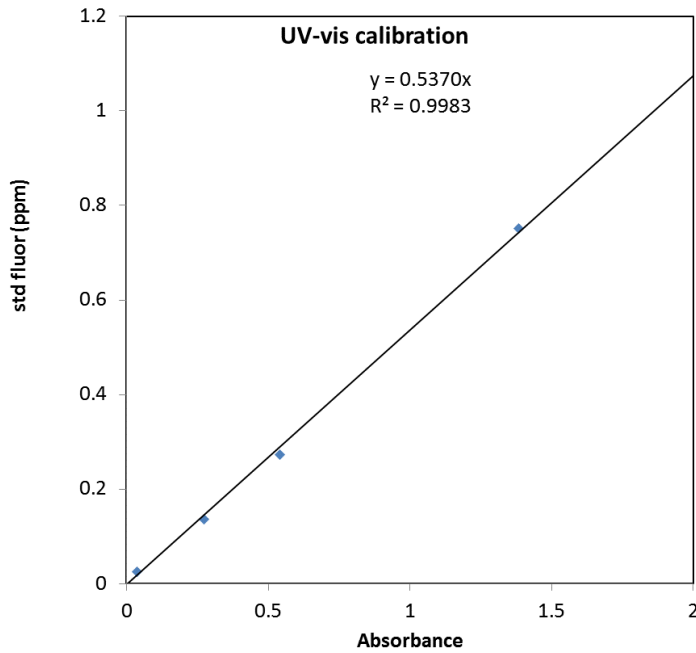


Figure 11: Example UV-Vis spectrophotometer calibration of fluorescein standards; concentration versus 494 nm absorbance.

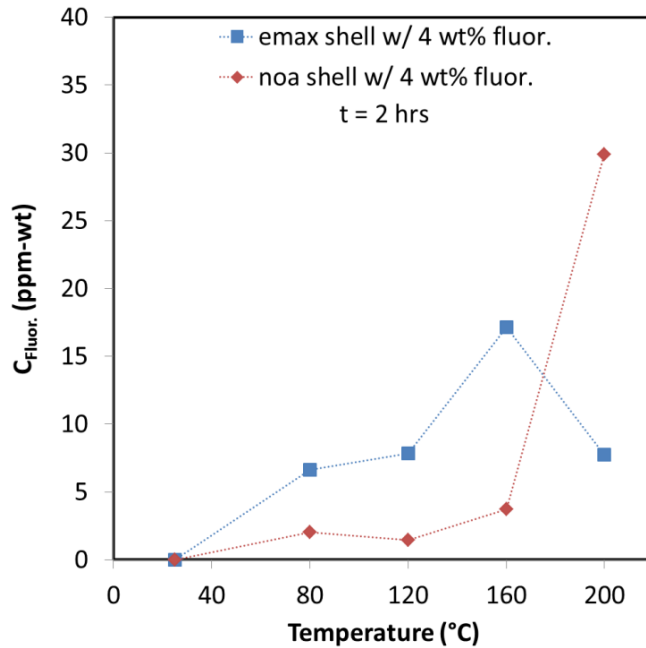


Figure 12: Fluorescein concentration in release test samples as a function of temperature for capsule shells of NOA (red diamonds) and E-MAX (blue squares).

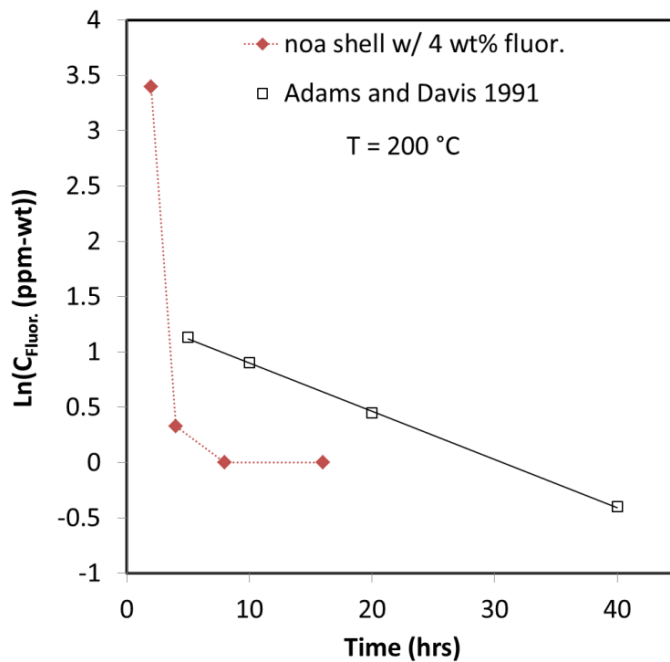


Figure 13: Fluorescein from NOA capsule release tests at 200 $^{\circ}\text{C}$ as a function of time (red diamonds). Measured fluorescein degradation in oxygenated water (Adams and Davis, 1991) is plotted for comparison (white squares).

Discussion

We successfully encapsulated a commonly used tracer in two shell materials, NOA and E-MAX, resulting in fairly uniform density and size distributions. The E-MAX capsules tended to collapse after curing but did not release inner tracer solution, whereas the NOA capsules remained relatively sturdy and spherical after fabrication (Figure 7). The capsules were mechanically durable and withstood handling and pumping through syringe pumps and tight fractures. The NOA capsules transported fairly easily through the fracture flow-cells because they were spherical and almost neutrally buoyant. When traveling horizontally these capsules mainly interacted with the lower fracture surface when fracture apertures exceeded the capsule diameter. For apertures lower than the capsule diameter, the capsules could still move through the fracture if fluid velocities were high enough to force capsules through irregular topographies. This forcible dislodgement resulted in some observable deformation but the capsules remained intact without rupturing. During vertical flow, entrained capsules moved upwards until interaction with prominent fracture features, at which point they cascaded downward until re-entrainment (Figure 8).

Fluorescein concentrations measured from capsule release tests are the product of two competing processes: release from capsules, and degradation due to oxidation (e.g., Adams and Davis, 1991). The capsule shell materials may also provide protection to the fluorescein from oxidative exposure, so long as the capsule remains impermeable. The relationship between temperature and fluorescein concentrations differed for the two capsule shell materials in the 2-hour release tests (Figure 12). At lower temperature, the E-MAX capsules released relatively higher amounts of fluorescein (7-17 ppm) than did the NOA capsules (2-4 ppm). At 200 °C, however, fluorescein concentrations from E-MAX capsules tests were much lower (8 ppm) than the 30 ppm levels noted for NOA capsules tests.

For E-MAX capsules, significant fluorescein release appears to have occurred at temperatures as low as 80 °C, suggesting that the glass transition temperature of the E-MAX (57 °C) has likely increased shell permeability, allowing some tracer release. The lower fluorescein concentration measured at the highest temperature (200 °C) likely resulted from enhanced fluorescein degradation at this temperature, rather than from lower rates of tracer release from the E-MAX shell. At this temperature, the majority of encapsulated fluorescein was likely released early on and subsequently degraded during the 2-hour test. In a ~16-hour test conducted at 200 °C, the E-MAX shells apparently continued reacting (evidenced by shell color change), but remained largely intact.

In contrast, the NOA capsules released very little fluorescein (2-4 ppm) in 2-hour tests at temperatures < 160 °C, suggesting that the NOA shells remained fairly impermeable (Figure 12). We suspect that low concentrations of fluorescein measured at temperatures < 160 °C reflect contributions from the capsule surfaces because of the lack of variability in concentration with temperature, but diffusion through the NOA shell may contribute as well. However, the large increase in fluorescein concentration (30 ppm) measured after a 2-hour, 200 °C test is attributable to rapid NOA dissolution at this temperature (noted at similar timescales in longer duration tests). The fluorescein also decays rapidly at 200 °C and is essentially undetectable after 4 hours (Figure 13).

Next Steps

Future work will be performed to attempt encapsulation and testing of naphthalene sulfonates, which are more stable than fluorescein at oxidizing, high-temperature conditions. In contrast to fluorescein, naphthalene sulfonates have been demonstrated to be thermally stable with no significant decay after 1 week at 330 °C (Rose et al., 2002). In addition, these compounds are environmentally benign with no known carcinogenic or mutagenic effects (Greim et al., 1994), and they are easy to detect via UV-Vis (Rose et al., 2001; 2002). Replacing fluorescein solutions with sodium naphthalene sulfonates solutions as the inner fluid is expected to be technically straightforward.

Further down-selection and design is needed to tailor capsule shell materials for geothermal applications. Ideally the shell would release tracer contents after hitting a discrete phase transition at a specific temperature, like the E-MAX; however, the temperature of release should be higher, like the NOA. There are numerous adhesive materials and compounds that are compatible with double emulsion devices and may be better candidates to meet the needs of this specific application. Smart tracers could also be designed to trigger by any variety of other physical and chemical conditions (Esser-Kahn, et al., 2011). In addition to temperature-sensing via encapsulated tracers, the ability to map other conditions within wellbores and fracture networks using a similar microcapsule approach would also be highly beneficial in enhancing oil and gas recovery efforts.

Acknowledgements

Thanks to Dustin Crandall and Dustin McIntyre (NETL) for providing XRCT data and Marcellus shale core via Susan Carroll (LLNL); Stuart Walsh and Dave Ruddle (LLNL) for help in designing and manufacturing the flow cells; Will Smith and T. Corzett (LLNL) for assistance in manufacturing capsules; Marcus Worsley (LLNL) for providing use of a pressure vessel; Sarah Baker (LLNL) for assistance with UV-Vis analyses; and Roger Aines (LLNL) for valuable comments and discussion. This work was performed under the auspices of the U.S. Department of Energy by Lawrence Livermore National Laboratory under Contract DE-AC52-07NA27344.

References

- Adams M. C. and Davis J. (1991) Kinetics of fluorescein decay and its application as a geothermal tracer. *Geothermics*, 20(1/2), 53-66.
- Alaskar M., Ames M., Connor S., Liu C., Cu Y., Li K., and Horne R. (2012) Nanoparticle and microparticle flow in porous and fractured media – An experimental study. In: *SPE Annual Technical Conference and Exhibition*, Denver, CO, 30 October – 2 November 2011, 1160-1171.
- Dennis B. R., Potter R., and Kolar J. (1981) Radioactive tracers used to characterize geothermal reservoirs, *Geothermal Resources Council Meeting*, 1-7.
- Esser-Kahn A. P., Odom S. A., Sottos N.R., White S. R., and Moore J. S. (2011) Triggered release from polymer capsules, *Macromolecules*, 44, 5539-5553.

- Greim H., Ahlers, R., Bias, R., Broecker, B., Hollander, H., Gelbke, H.P., Klimisch, H.J., Mangelsdorf, I., Paetz, A., Schon I., Stropp, G., Vogel, R., Weber, C., Ziegler-Skylakakis, K., and Bayer, E. (1994) Toxicity and ecotoxicity of sulfonic acids: Structure-activity relationship. *Chemosphere*, 28(12), 2203-2236.
- Gunderson R., Parini M., and Sirad-Azwar L. (2002) Fluorescein and naphthalene sulfonate liquid tracer results at the Awibengkok geothermal field, West Java, Indonesia. In: *Proceedings, 27 Workshop on Geothermal Reservoir Engineering*, Stanford University, Stanford, CA, USA, January 28–30, 2002, SGP-TR-171, 6 pp.
- Nottebohm M., Licha T., and Sauter M. (2012) Tracer design for tracking thermal fronts in geothermal reservoirs, *Geothermics*, 43, 37-44.
- Rose, P., Benoit, W.R., Kilbourn, P.M., 2001. The application of polyaromatic sulfonates as tracers in geothermal reservoirs. *Geothermics* 30, 617–640.
- Rose, P., Johnson, D.S., Kilbourn, P., Kastelen, C., 2002. Tracer testing at Dixie Valley, Nevada using 1-naphthalene sulfonate and 2,6-naphthalene disulfonate. In: *Proceedings, 27 Workshop on Geothermal Reservoir Engineering*, Stanford University, Stanford, CA, USA, January 28–30, 2002, SGP-TR-171, 6 pp.
- Shah R. K., Shum H. C., Rowat A. C., Lee D., Agresti J. J., Utada A. S., Chu L.-Y., Kim J.-W., Fernandez-Nieves A., Martinez C. J., and Weitz D. A. (2008) Designer emulsions using microfluidics. *Materials Today*, 11(4), 18-27.
- Tester J. W., Anderson B. J., Batchelor A. S., Blackwell D. D., DiPippo R., Drake E. M., et al. (2006) *The future of geothermal energy*. Massachusetts Institute of Technology, Cambridge, MA, USA, 372pp.
- Wu X., Pope G. A., Shook G. M., and Srinivasan S. (2005) A method of analyzing tracer data to calculate swept pore volume and thermal breakthrough in fractured geothermal reservoirs under two-phase flow conditions, In: *Proceedings, 30 Workshop on Geothermal Reservoir Engineering*, Stanford University, Stanford, CA, USA, January 31– February 30, 2002, SGP-TR-176, 7 pp.